Article

Advancing SilverSil sol-gel chemistry towards practical application

Giovanna Li Petri,[1] Rosaria Ciriminna,[1*] Mario Pagliaro[1*]

[1] Istituto per lo Studio dei Materiali Nanostrutturati, CNR, via U. La Malfa 153, 90146 Palermo, Italy

*Correspondence: rosaria.ciriminna@cnr.it, mario.pagliaro@cnr.it

SUMMARY

Showing significant antimicrobial activity (*in vitro*), SilverSil is the name of sol-gel coatings consisting of organically modified silica (ORMOSIL) entrapping silver nanoparticles originally derived from methyltriethoxysilane (MTES) and tetraethylorthosilicate (TEOS) only. In this study, we report the outcomes of investigation aimed at developing SilverSil coatings in sight of practical application. Besides MTES, we investigate the use of 3-(aminopropyl)trimethoxysilane (APTMS) to prepare new SilverSil coatings. The effect of selected parameters including the water/alkoxide ratio, the presence of ethanol as a co-solvent, the time of gel aging, the gel drying conditions, and the presence of $AgNO_3$ were investigated. Results are revealing and further support the investigation of SilverSil towards practical application as antibacterial coatings of broad scope and limited antimicrobial resistance.

Keywords: SilverSil, antibacterial, ORMOSIL, sol-gel coating, Ag nanoparticle

1 INTRODUCTION

Introduced in 2020, SilverSil is a broad scope antibacterial sol-gel material whose antibacterial activity so far has been demonstrated *in vitro* [1]. Consisting of organically modified silica (ORMOSIL) entrapping silver nanoparticles (NPs) originally derived from methyltriethoxysilane (MTES) and tetraethylorthosilicate (TEOS) [1]. Colloidal silver (i.e., silver NPs) is a powerful antimicrobial of broad scope and low toxicity whose mechanism of action minimizes antimicrobial resistance [2]. Accordingly, it comprises the active pharmaceutical ingredient of numerous antimicrobial commercial products widely used across the world since more than a century. Along with Albo and Trebelsi, we have suggested elsewhere that antimicrobial formulations based on microencapsulated Ag NPs will be amid next-generation antimicrobials [3].

Part of the numerous microencapsulation technologies developed so far, the sol-gel entrapment of metal nanoparticles in ORMOSIL matrices is particularly advantageous due to the pronounced chemical and physical stabilization of the entrapped nanoparticles; the lack of toxicity of the hybrid (organic-inorganic) organosilica material; and the unique versatility of the sol-gel process that allows to obtain the sol-gel doped material in virtually any shape (powder, film, thin coating, monolith etc.) [4].

When applied to kill harmful bacteria, Ag NPs penetrate the bacterial membrane and accumulate therein. Bacteria killed then act as reservoirs of bactericidal Ag NPs that are readily transferred to other bacteria, propagating the bactericidal effect [5].

This is particularly relevant in sight of practical applications of these coatings, because the hydrophilic-lipophilic balance of ORMOSIL can be widely tuned thanks to the unique versatility of silicon alkoxide chemistry [6], making these materials ideally suited for drug release [7]. In this study, we report the outcomes of sol-gel material chemistry research applied to the SilverSil class of materials in view of practical applications aimed at developing practically useful SilverSil coatings for a wide variety of applications. Along with that of MTES, we investigate the use of 3-(aminopropyl)trimethoxysilane (APTMS) to prepare new SilverSil coatings. In 2011, indeed, Chen and co-workers reported the excellent antibacterial performance of an ORMOSIL derived from TEOS and 3-(2-aminoethylaminopropyl)trimethoxysilane subsequently impregnated with Ag NPs [8].

Besides we investigate the preparation of new SilverSil coatings in the presence or without added $AgNO_3$ as well as the effect of selected parameters including the water/alkoxide ratio, the absence of ethanol as a co-solvent, the time of gel aging, and the alcogel/hydrogel drying conditions. Results are revealing and further support the investigation of SilverSil towards practical application as antibacterial coatings of broad-scope and limited antimicrobial resistance.

2. MATERIALS AND METHODS

2.1 Reagents

TEOS (purity grade >99%), MTES (purity grade >99%), APTMS (>99% pure), NaBH4 (purity grade 96%), aqueous nitric acid (65 wt%, purity grade >99%), aqueous ammonia (25 wt%), and $AgNO_3$ (>99.9% pure) were purchased from Sigma Aldrich (St. Louis, MI, USA). All chemicals were of high purity and were used without any further purification. MilliQ water (Barnstead Smart2Pure Water Purification System, Thermo Scientific) was used in all the sol-gel material syntheses.

2.2 SilverSil and blank ORMOSIL preparation

Doped SilverSil materials and their related blank (70% TEOS and 30% MTES, in molar terms, Table 1) were obtained by the sol-gel method (Figures 1a, 1b). In particular,

three sets of materials were prepared based on different gelation steps (Table 1): set A, including SilverSil 02,04,05,06 prepared according to the protocol reported previously [1]. SilverSil09 and SilverSil10, belonging to set B, were obtained by: *i*) suspending the alkoxide precursors in water instead of ethanol, *ii*) removing EtOH from alkoxide hydrolysis before the gelation step, and *iii*) drying the gel at room temperature (RT). Finally, set C (including SilverSil13,14,16b,19, and 20), was prepared with the same procedure as set B, but drying the gel in the oven at 70 °C.

In general, aqueous HNO_3 was added to catalyze the hydrolysis of alkoxides. In the case of blank material (no $AgNO_3$ added) a transparent and colourless gel was then obtained by adding ammonia bringing the pH to 8. Gelation occurred rapidly. The wet gel was then left to dry at RT or in the oven (3 days). The glassy monolith (Figure 1c) obtained was crushed into powder in a mortar with a pestle (Figure 1d). The blank SilverSil was extensively washed with water and then with a 50% (v/v) EtOH:H_2O solution, dried and sieved through the mesh of a laboratory sieve (aperture 150 µm, Cisa Sieving Technologies, Barcelona, Spain). In the case of SilverSil preparation, an aqueous solution of $AgNO_3$ was added to alkoxide mixture. Hydrolysis and gelation were promoted as in the case of the blank material. The resulting SilverSil xerogel was treated with an excess of $NaBH_4$ solution (1:100). The white suspension turned yellowish or brownish depending on the amount of $AgNO_3$ loaded (Figure 1e). The material was filtered through a glass microfiber filters (Whatman, Grade GF/B) and washed first with water, followed by washing with a 50% (v/v) EtOH:H_2O solution, dried in an oven at 40 °C, and finally sieved through a laboratory sieve with a 150 µm aperture. Figure 1f shows the SilverSil in a mortar after undergoing crushing with a pestle.

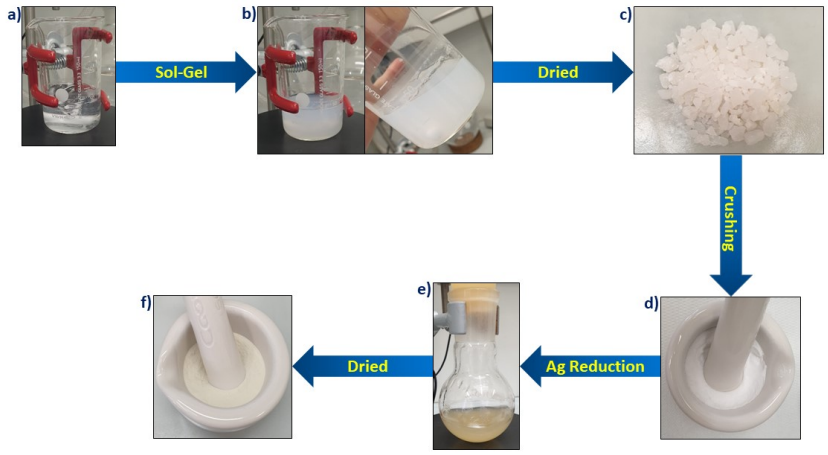

Figure 1. Workflow of sol-gel preparation of SilverSil xerogel: a,b) sol-gel transition; c) glassy-looking SilverSil after gel drying; d) crushed SilverSil powder before reduction of Ag^+; e) reduction of Ag^+ ions into Ag NPs; f) SilverSil powder doped with Ag NPs.

Figure 2 displays the blank ORMOSIL next to SilverSil xerogels of increasing Ag load.

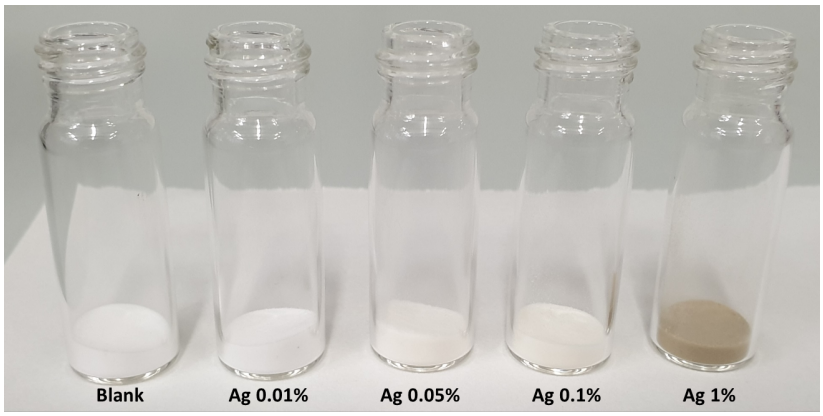

Figure 2. Representative image of SilverSil samples blank and doped with different $AgNO_3$ loadings (from left to right: blank and theoretical Ag NPs 0.01%, 0.05%, 0.1%, and 1%).

As mentioned above, three set of materials were prepared (Set A, B and C).

Set A materials (SilverSil04,02,05,06) were prepared as follows: in the case of SilverSil02,05 and 06 (Table 1) a solution of TEOS (3.94 mL, 17.8 mmol) and MTES (7.85 mL, 39.4 mmol) in 13.3 mL of absolute ethanol, was added with 6 mL of HNO_3 0.2 M dropwise under vigorously stirring at RT, followed after 10 min by APTMS (0.125 mL, 0.716 mmol). For the doped samples, an aliquot of $AgNO_3$ 6.36 mM (5 mL for SilverSil02, 2.5 mL for SilverSil05, and 0.5 mL for SilverSil06) was slowly added under stirring, followed by addition of ultrapure water to achieve the ratio reported in the Table 1. Gelling was carried out by adding 6 mL of aqueous ammonia 0.2 M dropwise under stirring. The wet gel was dried at RT for 30 days. A 1 g SilverSil precursor sample was suspended in 10 mL ultrapure water and stirred with a diluted solution of $NaBH_4$ 0.03 M (3.18, 1.59 and 0.318 mmol, for SilverSil02,05 and 06, respectively) for 1 h at RT. Hence, the suspension was filtered and the filtrate washed with 500 mL of water, followed by 200 mL of 50% (v/v) EtOH:H_2O solution, and finally dried in an oven at 40 °C for approximately 5 h.

Set B materials (SilverSil09,10) were prepared as follows: a mixture of TEOS (3.94 mL, 17.8 mmol) and MTES (7.85 mL, 39.4 mmol) in 13.3 mL ultrapure water, was added with 6 mL of HNO3 0.2 M dropwise under vigorous stirring at RT. After 10 min, the mixture turned into a solution. The latter solution was added with APTMS (0.125 mL, 0.716 mmol) and left under stirring for 1 h at RT. Ethanol released via alkoxide hydrolysis was removed under reduced pressure (125 mbar) and replaced with the same volume (11 mL) of ultrapure water. In the case of SilverSil10 an aliquot of 5 mL of $AgNO_3$ 6.36 mM was slowly added, followed by 5 ml of water. For the blank material SilverSil09, the aliquot of $AgNO_3$ was replaced with water (5 mL), followed by the aliquot of water to achieve the ratio in Table 1. Gelling occurred by adding 3 mL of aqueous ammonia (0.2 M) dropwise. The hydrogel was dried at RT for 30 days. In the case of SilverSil10, a 1 g sample of the precursor material doped with AgNO3 was suspended in 10 mL ultrapure water. The dispersion was added with a diluted solution of $NaBH_4$ 0.03 M (3.18 mmol) and left under stirring for 1 h at RT. The xerogel suspension was filtered and the filtrate washed with 500 mL of water, followed by 200 mL of 50% (v/v) EtOH:H_2O solution. The washed xerogel was dried in an oven at 40 °C for approximately 5 h.

Set C materials (SilverSil13,14,19,20,16b) were prepared as follows: a dispersion of TEOS (3.94 mL, 17.8 mmol) and MTES (7.85 mL, 39.4 mmol) in 13.3 mL of ultrapure

water was added with 6 mL of HNO_3 0.2 M dropwise under vigorous stirring at RT. After 10 min, the dispersion turned into a solution and APTMS (0.125 mL, 0.716 mmol) was added leaving the solution under stirring for 1 h at RT. EtOH originating from the hydrolysis of alkoxides was removed under reduced pressure (125 mbar) and replaced with the same volume (11 mL) of water. In the case of SilverSil14,19,20, an aliquot of $AgNO_3$ 6.36 mM (5 mL for SilverSil14, 2.5 mL for SilverSil19, and 0.5 mL for SilverSil20) was added dropwise, followed by the aliquot of ultrapure water to achieve the ratio reported in Table 1.

Table 1. SilverSil samples by load, gel treatment, EtOH:alkoxide and H_2O/alkoxide ratio.

Ag (% theor.)	Gel treatment	EtOH/TEOS	EtOH/MTES	H_2O/TEOS	H_2O/MTES
Set A					
0.0	Dried at RT for 30 days	23.4	11	68.6	31
0.1	Dried at RT for 30 days	23.4	11	68.6	31
0.05	Dried at RT for 30 days	23.4	11	68.6	31
0.01	Dried at RT for 30 days	23.4	11	68.6	31
Set B					
0.0	Dried at RT for 30 days	0	0	135	62
0.1	Dried at RT for 30 days	0	0	135	62
Set C					
0.0	Aging 48h, dry at 70 °C	0	0	135	62
0.1	Aging 48h, dry at 70 °C	0	0	135	62
1	Aging 48h, dry at 70 °C	0	0	135	62
0.05	Aging 48h, dry at 70 °C	0	0	135	62
0.01	Aging 48h, dry at 70 °C	0	0	135	62

In the case of SilverSil16b, a portion (7.95 mL) of a solution $AgNO_3$ 40 mM was added, followed by an aliquot of ultrapure water (2.05 mL) in order to maintain the same water/alkoxides ratio. In the case of the blank material SilverSil13, the aliquot of $AgNO_3$ was replaced with water. Gelling occurred by adding 3 mL of aqueous ammonia 0.2 M dropwise. The wet hydrogel was aged for 48 h at RT and then dried in an oven at 70 °C for 3 days. A 1 g sample of the SilverSil xerogel precursor doped with $AgNO_3$ was suspended in 10 mL ultrapure water (in 20 mL, in the case of

SilverSil16b) and added under stirring a solution of NaBH4 0.03 M (3.18, 1.59, 0.318, and 31.8 mmol for SilverSil14, 19, 20, and 16b, respectively) for 1 h a RT. Finally, the suspension was filtered and washed with 500 mL of water, followed by 200 mL of 50% (v/v) EtOH:H_2O solution. The washed xerogel was dried in an oven at 40 °C for approximately 5 h.

2.2 Materials characterization

The FTIR spectra were recorded with a Fourier-Transform Infrared Spectrophotometer (Bruker, Billerica, MA, USA) in the measuring range 400 – 4000 cm^{-1}, with a lateral resolution of 4 cm^{-1} and 128 scans per sample. All material powders were mixed with the ultrapure KBr (FTIR grade, ≥ 99% pure, Sigma-Aldrich) at weight ratio (mg) of 100:1, using a pestle and mortar. The finely obtained mixture was molded into a disc shape using a Specac Mini-Pellet laboratory hydraulic press applying a 12 t.

The X-ray diffraction (XRD) measurements were obtained using a D5005 X-ray diffractometer (Bruker AXS, Karlsruhe, Germany) operating at 40 kV and 30 mA. The diffraction profile was obtained at a 0.15°/min acquisition rate, spanning a 10.0°–80.0° 2θ range. The X-ray radiation, generated through a copper (Kα) anode, was rendered monochromatic via the instrument's secondary monochromator.

The ζ-Potential analysis was performed using a Malvern Zetasizer Nano ZS (Malvern Panalytical, Malvern, Great Britain) equipped with a He-Ne laser at a power of 4.0 mW operating at a wavelength of 633 nm. Before the measurements, all samples were sifted with a mesh sieve of 150 µm, and a suspension was prepared in ultrapure water (5 mg/1 mL) maintaining the pH of 7.4 during the measurement carried out in a folded capillary cell (Malvern ZETASIZER NANO SERIES).

Surface information about materials including the specific surface area (SSA), specific pore volume (SPV) and pore size distribution, were assessed from the adsorption-desorption isotherms of cryogenic N_2 as the adsorbate using the Quantachrome (Boynton Beach, FL, USA) NOVA 2000e material analyzer. Prior to analysis, the sample underwent degassing under vacuum at 200 °C for 120 min. The SSA of the samples was determined utilizing the multipoint Brunauer-Emmett-Teller (BET) model, employing the average adsorption and desorption values of relative pressure P/P_o within the range of 0-0.98 at the fixed temperature of 77.4 K. The pore size distribution and PSV were calculated by applying the Barrett-Joyner-Halenda (BJH) model to the desorption branch of the isotherms across the whole P/P_o range. The experimental data and graph were processed using OriginPro software, version 2024 (OriginLab, Northampton, MA, USA).

3. RESULTS AND DISCUSSION

The FTIR spectra in Figure 3 of both blank and SilverSil materials doped with Ag^+ or with metal nanoparticle Ag^0 show the typical bands in the 950–1250 cm^{-1} region which corresponds to the silica structural fingerprint, the ν_{as}Si-O-Si mode, split in two observable components, with maxima at ~1130 and ~1050 cm^{-1} corresponding to the longitudinal and transverse optical components (LO and TO, respectively) of different siloxane rings: six-member $[(SiO)_6]$ and four-member $[(SiO)_4]$ [9]. The signals at 920 cm^{-1} and 779 cm^{-1} are, respectively, those of Si-OH stretching, and symmetric ν_sSi-O-Si vibration mode.

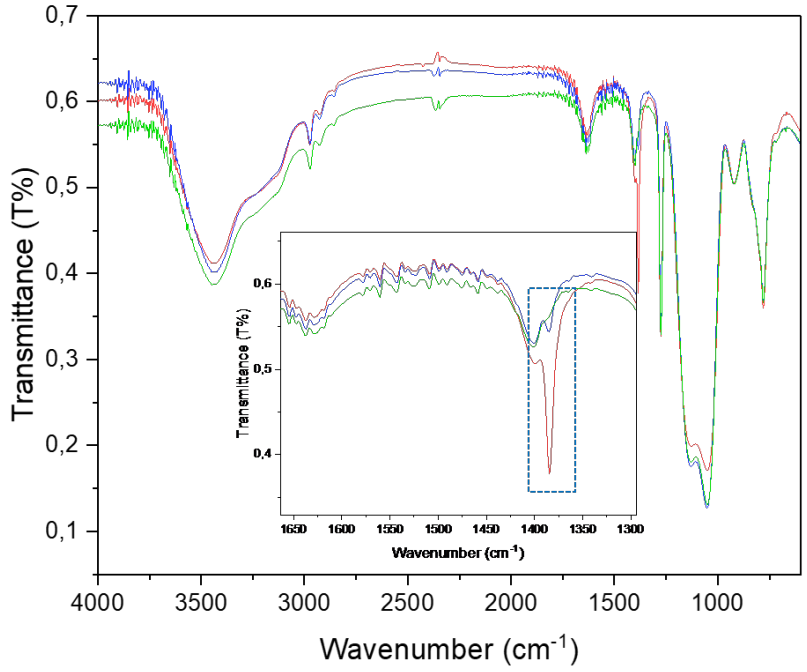

Figure 3. Representative FTIR spectra of blank SilverSil09 (blue line), and doped SilverSil10 before (red line) and after (green line) reduction with $NaBH_4$.

A broad common band centered at 3438 cm^{-1}, characteristic of O-H stretching vibrations is due to water adsorption air together with the O-H bending signal at around 1640 cm^{-1} [10]. However, this band is superimposed to the N-H stretching vibration of the NH_2 functional group of APTMS, and with that of residual silanol groups (Si–OH) located at the surface of the silica particles. Peaks at 2971 and 2922 cm^{-1} are relative to the stretching vibrations of C-H bonds of aliphatic -CH_2 propyl amino chain, that are overlapped with the antisymmetric and symmetric, respectively, stretching modes of the methyl group bound to the Si atom [11]. The Si-CH_3 group is also recognized by a strong and sharp band at 1270 cm^{-1}.

The SilverSil material (SilverSil10 before reduction with NaBH4) entrapping the Ag+ ions not yet reduced to Ag^0 nanoparticles shows a sharp and intense absorption band at 1385 cm^{-1} due to the C-N stretching vibration [12] that is significantly stronger compared to blank material due to possible signals overlap: the asymmetric N–O stretching in the NO_3^- group [13]; and the increased C-N stretching due to the interaction of the positive charge of Ag^+ with the electron-pair donors of NH_2 functional groups [14]. This interaction keeps the silver species highly dispersed and may hinder the growth of Ag NPs into large metal clusters during the reduction step. Remarkably, the peak at 1385 cm^{-1} completely disappears after reduction of Ag+ ions into metal species. In other words, the strong interaction between the amine group of APTES and the Ag NPs at the surface of the sol-gel cages dramatically reduces the C-N stretching vibration.

The XRD patterns in Figure 4 confirm the amorphous structure of the SilverSil and blank ORMOSIL materials (the blank SilverSil04) and doped SilverSil14 and SilverSil16b. The broad peak centered at $2\theta \approx 23°$ pointing to the Bragg d-spacing of 9.61 Å originating from the constant nearest silicon atoms in the siloxane Si–O–Si units in the xerogel matrix [15].

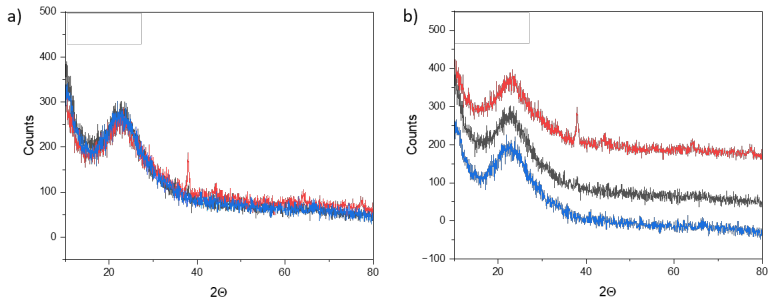

Figure 4. a) Stacked and b) unstacked XRD pattern of SilverSil14 (black curve), SilverSil16b (red curve) and SilverSil04 (blue curve).

No other diffraction peaks at higher angles are observed in SilverSil14 (0.0318 mmol of AgNO3 used in the preparation) likely due to the low concentration, as reported with the original work introducing the SilverSil class of materials [1]. In contrast, the Ag metal X-ray diffraction pattern is evident for the SilverSil16b material in which the amount of AgNO3 added during the material sol-gel synthesis was ten times higher (0.318 mmol). In this case, the XRD pattern shows the presence of diffraction peaks at 37.9°, 44.4° and 64.2° corresponding to the (111), (200) and (220) planes of crystalline Ag, respectively [16].

Insights into the stability and surface charge of the SilverSil microparticles dispersed in water at neutral pH were obtained through ζ-potential measurement. The analysis clearly revealed a localization of positive charges on the surface of the silica microparticles, both in blank and doped SilverSil materials (Table 2).

Table 2. ζ potential values of SilverSil samples measured at pH 7

Material	ζ -potential (mV)
SilverSil02	22.4 ± 5.43
SilverSil04 (blank)	27.5 ± 4.78
SilverSil05	23.1 ± 5.56
SilverSil06	24.9 ± 5.61
SilverSil09 (blank)	31.6 ± 6.41
SilverSil10	21.8 ± 4.71
SilverSil13 (blank)	24.8 ± 6.29
SilverSil14	19.8 ± 3.37
SilverSil16b	18.5 ± 4.04
SilverSil19	18 ± 7.37
SilverSil20	18.6 ± 7.68

Overall, all doped SilverSil materials show lower ζ-potential values, ranging from 18 to 24.9 mV. The silver-free blank samples have higher ζ-potential values, ranging from 24.8 to 31.6 mV, regardless the method of preparation. This difference once again points to the strong interaction of $–NH_2$ groups at the surface of the SilverSil microparticles and the Ag NPs at the surface of the sol-gel cages. The interaction reduces the amount of NH_3^+ groups formed in the aqueous phase upon hydrolysis of the $-NH_2$ groups pending the outer surface of the SilverSil material.

Finally, the isotherms in Figure 5 show the mesoporous nature of SilverSil materials with pore size less than 20 nm and adsorption-desorption isotherms of intermediate between type-IV and type-II, with hysteresis loops close to type H1, characteristic of

capillary condensation in open cylindrical mesopores between spheroidal particles of fairly uniform array [17], large SSA and PSV.

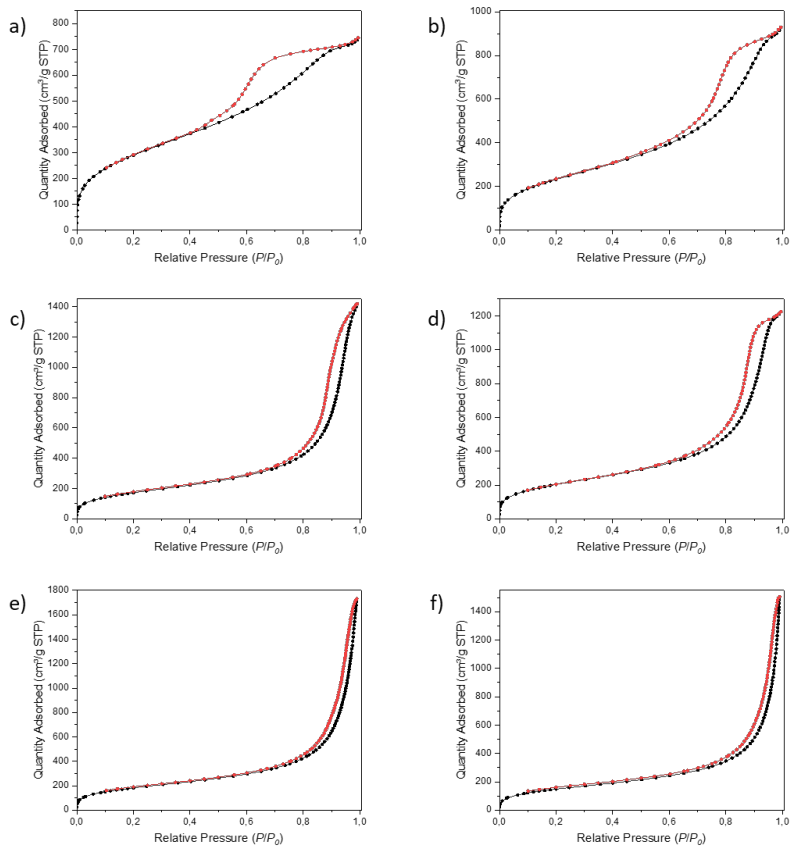

Figure 5. N_2 adsorption/desorption isotherms linear plot of; *top*) SilverSil04 (a) and SilverSil02 (b); *middle*) SilverSil09 (c) and SilverSil10 (d); *bottom*) SilverSil13 (e) and SilverSil14 (f).

The method of preparation influenced SSA, PSV, and pore size values.

Table 3. Specific surface area (SSA), pore specific volume (PSV), and pore size of SilverSil materials.

Samples	SSA (m^2/g)	PSV (cm^3/g)	Pore size (nm)
SilverSil04 (blank)	1,062	1.10	4.37
SilverSil02	857	1.48	6.31
SilverSil05	748	1.26*	7.44**
SilverSil06	1,088	1.41	5.42
SilverSil09 (blank)	640	2.17	14.09
SilverSil10	747	1.86	10.69
SilverSil13 (blank)	674	2.63	17.41
SilverSil14	551	2.29	18.33

*BJH Adsorption cumulative volume of pores; **BJH Adsorption average pore width.

The blank SilverSil04 (1,062 m^2/g) and its doped analogue SilverSil02 (857 m^2/g) show the high values of SSA, and type-IV adsorption-desorption isotherms (Figure 5a and b, respectively). High slopes were observed for the adsorption isotherms of

SilverSil13 and SilverSil14 at relative pressure (P/P0) above 0.9 (Figure 5e and f, respectively). For these materials, drying was conducted in the absence of ethanol (removed under vacuum). On the other hand, SilverSil09 and its doped analogue SilverSil10 showed intermediate slopes (Figure 5c and d, respectively). This observation suggests that in the absence of EtOH, drying the hydrogel at RT or in an oven drives formation of larger pores [18] (see pore size trend in Table 3).

In addition, the higher SSA values for SilverSil samples gelled in the presence of higher amounts of EtOH and dried at room temperature (SilverSil02, 04, 05, and 06) is due to lower capillary forces at the surface of the as-formed sol-cages during evaporation at room temperature of the aqueous ethanol liquid phase. Prolonged and gradual drying at RT promotes reduced shrinkage of the alcogels compared to the drying at 70 °C.

4. CONCLUSIONS

In conclusion, the study of SilverSil glasses obtained through a two-step sol-gel hydrolytic polycondensation process of TEOS and organically modified silanes MTES and APTMS in the presence or without added $AgNO_3$ following the preparation route reported in the literature [1] or modified in selected parameters including the water/alkoxide ratio, the absence of ethanol as a co-solvent, the time of gel aging, and the drying conditions of the gels, reveals numerous aspects that will be instrumental towards the first practical application of this promising class of sol-gel materials.

First, the amine functional group of APTMS functions as a stabilizer of silver atom clusters during reduction step, preventing aggregation into larger particles [19].

Second, the highest encapsulation efficiency of Ag NPs was found for the materials in which ethanol, used both as a co-solvent and derived from the silane hydrolysis, was removed prior to the gelling step. Probably, ethanol reduces the added Ag+ ions before the gelation step, leading to the formation of Ag NPs especially in the presence of aqueous ammonia as in the present case that acts as a reducing accelerator and even affects the nanoparticle morphology [20], eventually causing silver loss in the subsequent steps.

Third, the gel drying step also substantially influences the Ag nanoparticle encapsulation efficiency. Slow drying of the gels, even in the absence of ethanol, translated into lower encapsulation efficiency likely due to migration of Ag+ to the outer surface of the sol-gel cages of the xerogel from which some Ag NPs are partly lost during the reduction step and subsequent washing step.

All these findings will now be used to prepare optimal SilverSil coatings with which to functionalize textiles [21] and produce stable garments with prolonged antibacterial activity hopefully able to resist prolonged washing cycles of the textiles.

ACKNOWLEDGMENTS

We acknowledge funding supporting the work of G.L.P. via the Made in Italy - Circular and Sustainable (MICS) Extended Partnership funded by the European Union NextGenerationEU (PNRR - Missione 4, Componente 2, Investimento 1.3 – D.D. 1551.11-10-2022, PE00000004).

CONFLICT OF INTERESTS

There are no conflicts to declare.

REFERENCES

1. K. Trabelsi, R. Ciriminna, Y. Albo, M. Pagliaro, SilverSil: a new class of antibacterial materials of broad scope, *ChemistryOpen* **2020**, *9*, 459-463. DOI: 10.1002/open.202000016
2. S. Tang, J. Zheng, Antibacterial activity of silver nanoparticles: structural effects, *Adv. Healthcare Mater.* **2018**, *7*, 1701503. DOI: 10.1002/adhm.201701503
3. R. Ciriminna, Y. Albo, M. Pagliaro, New antivirals and antibacterials based on silver nanoparticles, *ChemMedChem* **2020**, *15*, 1619-1623. DOI: 10.1002/cmdc.202000390
4. D. Avnir, Organic chemistry within ceramic matrixes: doped sol-gel materials, *Acc. Chem. Res.* **1995**, *28*, 328-334. DOI: 10.1021/ar00056a002
5. R. K. Wakshlak, R. Pedahzur, D. Avnir, Antibacterial activity of silver-killed bacteria: the "zombies" effect, *Sci. Rep.* **2015**, *5*, 9555. DOI: 10.1038/srep09555
6. I. Roy, P. Kumar, R. Kumar, T. Y. Ohulchanskyy, K.-T. Yong, P. N. Prasad, Ormosil nanoparticles as a sustained-release drug delivery vehicle, *RSC Adv.* **2014**, *4*, 53498-53504. DOI: 10.1039/c4ra10293B
7. A. Fidalgo, R. Ciriminna, L. M. Ilharco, M. Pagliaro, Role of the alkyl-alkoxide precursor on the structure and catalytic properties of hybrid sol-gel catalysts, *Chem. Mater.* **2005**, *17*, 6686-6694. DOI: 10.1021/cm051954x
8. K.H. Wu, C.I. Liu, C.C. Yang, G.P. Wang, C.M. Chao, Preparation and characterization of aminosilane-modified silicate supported with silver for antibacterial behavior, *Mater. Chem. Phys.* **2011**, *125*, 802-806. DOI: 10.1016/j.matchemphys.2010.09.055
9. A. Fidalgo, R. Ciriminna, L. Lopes, V. Pandarus, F. Béland, L. M. Ilharco, M. Pagliaro, The sol-gel entrapment of noble metals in hybrid silicas: a molecular insight, *Chem. Centr. J.* **2013**, *7*, 161. DOI: 10.1186/1752-153X-7-161
10. S. Duhan, N. Kishore, P. Aghamkar, S. Devi, Preparation and characterization of sol–gel derived silver-silica nanocomposite, *J. Alloys Compd.* **2010**, *507*, 101-104. DOI: 10.1016/j.jallcom.2010.07.107
11. S. Y. Lin, S. T. Chang, Variations of vibrational local modes and electronic states of hydrogenated amorphous silicon carbide under thermal annealing, *J. Phys. Chem. Solids* **1998**, *59*, 1399-1405. DOI: 10.1016/S0022-3697(98)00236-4
12. N.B. Kondrashova, A. S. Shamsutdinov, V. A. Valtsifer, Surface modification of magnetic mesoporous systems with aminopropyl groups and their properties, *J. Inorg. Organomet. Polym.* **2021**, *31*, 1347-1358. DOI: 10.1007/s10904-020-01775-4
13. A.Tăbăcaru, C. Pettinari, M. Bușilă, R. M. Dinică, New antibacterial silver(I) coordination polymers based on a flexible ditopic pyrazolyl-type ligand, *Polymers* **2019**, *11*, 1686. DOI: 10.3390/polym11101686
14. P. Taba, P. Budi, A. A. Gau, Y. Hala, St. Fauziah, I. W. Sutapa, J. Manga, Mesoporous silica modified with amino group (NH_2-MCM-48) as adsorbent of Ag(I) and Cr(III) in water, *Rasayan J. Chem.* **2021**, *14*, 204-211. DOI: 10.31788/RJC.2021.1415963
15. S. L. B. Lana, A. B. Seddon, X-Ray diffraction studies of sol-gel derived ORMOSILs based on combinations of tetramethoxysilane and trimethoxysilane, *J. Sol–Gel Sci. Technol.* **1998**, *13*, 461-466. DOI: 10.1023/A:1008685614559
16. T. Thirugnanasambandan, M. Alagar, Electrolytic synthesis and characterizations of silver nanopowder, *Nano Biomed. Eng.* **2012**, 4, 58-65. DOI: 10.5101/nbe.v4i2.p58-65
17. S. J. Gregg K.S.W. Sing, *Adsorption, Surface Area, and Porosity*. Academic Press, New York **1982**.
18. Q. Chen, Y. Ge, H. Granbohm, S.-P. Hannula, Effect of ethanol on Ag@mesoporous silica formation by *in situ* modified Stöber method, *Nanomaterials* **2018**, *8*, 362. DOI: 10.3390/nano8060362

19. H. J. Hah, S. M. Koo, S. H. Lee, Preparation of silver nanoparticles through alcohol reduction with organoalkoxysilanes, *J. Sol-Gel Sci. Technol.* **2003**, *26*, 467-471. DOI: 10.1023/A:1020710307359
20. Y. Lee, S.-G. Oh, Ostwald ripening and control of Ag ion reduction degree by ammonium hydroxide in alcohol reduction process, *J. Ind. Eng. Chem.* **2015**, *21*, 768-771. DOI: 10.1016/j.jiec.2014.04.010
21. R. Ciriminna, Y. Albo, M. Pagliaro, Sol-gel nanocoatings to functionalize fibers and textiles: a critical perspective, *ChemistrySelect* **2020**, *5*, 9776-9780. DOI: 10.1002/slct.202001897